The Substructure of Isolated and In Situ Outer Dynein Arms of Sea Urchin Sperm Flagella

WINFIELD S. SALE, URSULA W. GOODENOUGH, and JOHN E. HEUSER
Department of Anatomy and Cell Biology, Emory University School of Medicine, Atlanta, Georgia 30322; and Departments of Biology and Cell Biology–Physiology, Washington University, St. Louis, Missouri 63110

ABSTRACT   Outer-arm dynein from the sperm of the sea urchin *S. purpuratus* was adsorbed to mica flakes and visualized by the quick-freeze, deep-etch technique. Replicas reveal particles comprised of two globular heads joined by two irregularly shaped stems which make contact along their length. One head is pear-shaped (18.5 × 12.5 nm) and the other is spherical (14.5-nm diam). The stems are decorated by a complex of bead-like subunits. The same two-headed protein is found in the 21S dynein-1 fraction of sucrose gradients. The β-heavy chain/intermediate chain 1 (beta/IC-1) dynein subfraction, produced by low-salt dialysis and zonal centrifugation of the high-salt-extracted dynein-1, contains only single-headed molecules with single stems. These heads are predominantly pear-shaped (18.5 × 12.5 nm). Since 21S dynein-1 contains two heavy chains (α and β), and the beta/IC-1 subfraction is comprised of only the β-heavy chain (Tang et al., 1982, *J. Biol. Chem.* 257:508–515), we conclude that each head is formed by a heavy chain, that the pear-shaped head contains the β-heavy chain, and that the spherical head contains the α-heavy chain. The in situ outer dynein arms of demembranated sperm were also studied by the quick-freeze, deep-etch method. When frozen in reactivation buffer devoid of ATP, each arm consists of a large globular head that attaches to the A-microtubule by distally skewed subunits and attaches to the B-microtubule by a slender stalk. In ATP, this head shifts its orientation such that it can be seen to be constructed from two globular domains. We offer possible correlates between the in situ and the in vitro images, and we compare the structure of sea-urchin dynein with dynein previously described from *Chlamydomonas* and *Tetrahymena*.

Dynein ATPases comprise the arms that project from the A-microtubule of the peripheral doublets of ciliary and eucaryotic flagellar axonemes (reviewed in references 14, 20, 27, 29, 31), and the dynein arms are believed to couple the binding and hydrolysis of ATP to structural changes that result in sliding between adjacent doublet microtubules (12, 17, 41, 49, 54, 56–58). Microtubule sliding, in turn, is the underlying basis for ciliary and flagellar bending (8, 45, 47, 48, 52, 53), although it is still unclear how sliding is converted into a propagated bend. In addition to its role in generating ciliary movement, there is evidence that dynein is involved in generating movements associated with other microtubule arrays such as the mitotic spindle (9, 23, 24, 39, 42, 43, 50).

The outer dynein arms from sea urchin sperm tails have been extensively studied (5). These proteins can be selectively solubilized by exposure to 0.6 M salt-containing buffers (7).

Such high-salt extracts contain an ATPase that sediments at 21S (21S dynein-1) and has a mass of 1.25 megadaltons (15). The partially purified 21S dynein-1 can restore functional outer arms to outer arm–depleted sperm axonemes (13). Since the 21S dynein-1 is both necessary and sufficient for such restoration, it has been concluded that 21S dynein-1 is the outer dynein arm (13). Each 21S dynein-1 is comprised of at least nine different polypeptides including the α- and β-heavy chains, the intermediate chains (IC)[1] 1, 2, and 3, and at least four light chains (6).

Each 21S dynein-1 has been shown to be a heterodimer of the α- and β-heavy chains. Exposure to low-salt conditions

---

[1] *Abbreviations used in this paper:* beta/IC-1, β-heavy chain/intermediate chain 1; D-foot, distal foot; IC, intermediate chain; P-foot, proximal foot.

converts 21S dynein-1 into three smaller particles: a 12–14S particle comprised of the β-heavy chain and intermediate chain 1 (beta/IC-1); a variably sized aggregate comprised of the α-heavy chain; and a 9–10S particle comprised of IC-2 and -3 (55). Both the α-heavy chain fraction and the beta/IC-1 were found to contain ATPase activity, and re-formation of the 21S dynein-1 required a mixture of all three of these subfractions (55). The reconstituted 21S dynein-1 always contained equal amounts of the α- and β-heavy chains. Moreover, Bell (3) found that the purified β-heavy chain has a mass of ~450 kD. It was therefore concluded that the 1.25-kD 21S dynein-1 complex is comprised of a single copy of each of the α- and β-heavy chains, and therefore two distinct ATPase domains, a model presented in detail by Bell and Gibbons (4).

To test the structural predictions of Bell and Gibbons (4), we have studied 21S dynein-1, its subfractions, and the in situ outer arms by the quick-freeze, deep-etch, rotary-shadow method of electron microscopy (19), an approach that has successfully revealed the substructure of isolated and in situ dyneins derived from protozoa (17–19, 56). We document that each 21S dynein-1 is indeed a two-headed molecule: one head is pear-shaped and is comprised of the β-heavy chain; the other head is spherical and is presumably comprised of the α-heavy chain. The disposition of this protein in situ and its conformational changes after ATP exposure are described.

MATERIALS AND METHODS

High-Salt Extraction of Dynein-1: Axonemes from the sperm tails of the sea urchin *S. purpuratus* were isolated by the method of Gibbons and Fronk (15). Sperm were homogenized in ~4 vol of a buffer composed of 5 mM imidazole, 0.1 M NaCl, 4 mM $MgSO_4$, 1 mM dithiothreitol, 5 mM 2-mercaptoethanol, 0.2 mM phenylmethylsulfonyl fluoride, and 0.5% Triton X-100. The homogenate was centrifuged twice at 2,000 g for 5 min to remove sperm heads. Axonemes were collected by pelleting at 12,000 g for 8 min, and washed twice in the buffer described above lacking Triton X-100 (wash buffer). The protein concentration of the axoneme suspension was determined, and the final pellet of axonemes was resuspended to 2 mg/ml in a high-salt buffer (0.6 M NaCl, 4 mM $MgSO_4$, 0.1 mM EDTA, 1 mM dithiothreitol, 5 mM 2-mercaptoethanol, 0.2% phenylmethylsulfonyl fluoride, 10 μM taxol, and 5 mM imidazole/HCl, pH 7.0) for 15 min on ice. The extracted axonemes were sedimented at 30,000 g for 20 min and the resulting supernate, referred to as the high-salt extract, was used for further experiments. Thin-section electron microscopy of axonemal cross-sections revealed that outer dynein arms were selectively extracted by high-salt treatment (data not shown).

Purification and Fractionation of Dynein-1: 21S Dynein-1 was partially purified from the high-salt extract by zonal centrifugation on 5–20% (wt/vol) sucrose gradients usually made up with the high-salt buffer as described above (55). The ATPase peak fraction was rapidly determined as described in Tang et al. (55), and peak fractions were prepared for SDS gel electrophoresis and electron microscopy as described below.

For preparation of the beta/IC-1 dynein-1 subunit, the high-salt extract was dialyzed against a low-ionic-strength solution containing 5 mM imidazole, pH 7.0, 0.5 mM EDTA, and 7 mM 2-mercaptoethanol for 15 h at 4°C. The beta/IC-1 subunit was isolated by zonal centrifugation as described in Tang et al. (55). Peak ATPase fractions were prepared for SDS gel electrophoresis and electron microscopy. Approximate sedimentation rates for all gradients were determined by the method of Martin and Ames (33) using catalase (11.3S), thyroglobin (19S), and latent activity dynein-1 (21.4S) as standards. (The 21S dynein-1 of the sea urchin sperm of *T. gratilla* was the generous gift of Dr. I. R. Gibbons, University of Hawaii.)

Electron Microscopy: Dynein molecules were analyzed using the quick-freeze, deep-etch, rotary-shadowing technique (18, 19, 22, 46). This involved placing a small volume (10–20 μl) of dilute protein solution (20 μg/ml) onto the surface of finely ground mica flakes that were supported by a thin slice of aldehyde-fixed lung. Just before freezing, the high-salt-extracted dynein-1 was diluted in buffer such that the final NaCl concentration was adjusted to 200 mM and the protein concentration to 20 μg/ml. For gradient-purified samples of 21S dynein-1 and the beta/IC-1 subunit, the sucrose was removed by a 6–8 h dialysis against the buffer utilized in the gradient, and the salt concentration was adjusted to 200 mM NaCl just before freezing. Lower final ionic strength resulted in less efficient adsorption of these proteins to the mica (data not shown, see reference 22). After 15 s of exposure to the mica, excess solution was drawn off, and the damp paste of mica was abruptly applied to a liquid helium–cooled copper block. The frozen mica samples were then freeze-fractured in a Balzers device (Balzers, Hudson, NH) and deep-etched at −95°C for 4 min, which sublimes away ~250 nm of ice and exposes the surfaces of a large number of mica flakes. Molecules adsorbed to these mica flakes were rotary-replicated with a thin layer of platinum (~1.5 nm, based on estimate from quartz thin film monitor) evaporated from a relatively shallow angle (10°), and the flakes were held together by depositing a thick layer of carbon (10-s evaporation during sample rotation). Replicas were separated from mica by immersion in concentrated hydrofluoric acid, cleaned, and picked up on standard grids. Control experiments included study of replicas of buffer devoid of proteins, of serial dilutions of proteins, and of other, non-dynein proteins (22).

Isolated axonemes or demembranated reactivated sperm (see below) were prepared for electron microscopy by the quick-freeze, deep-etch method described by Goodenough and Heuser (17). This involved collection of axonemes or demembranated sperm by centrifugation, rapid transfer of the pellet onto a slice of lung, and abrupt freezing on a liquid helium–cooled copper block. Isolated axonemes were frozen in wash buffer, and demembranated sperm were frozen in the reactivation buffer described below. The frozen samples were then fractured in the Balzers freeze-fracture machine, etched for 3 min at −105°C, and rotary-replicated with platinum applied from a 24° angle. Replicas were cleaned in bleach and picked up on standard grids.

Replicas were viewed with JEOL 200CX or JEOL 100CX transmission electron microscopes (JEOL USA, Peabody, MA) operating at 100 kV. Representative mica flakes were photographed at 68,000×, in stereo, using ±10° of tilt with a eucentric side-entry goniometer stage. Magnification was strictly and repeatedly calibrated by stereophotography of negatively stained tropomyosin tactoids. Negatives were studied directly in three dimensions using a Wild APT-1 stereo map reader (Wild Heerbrugg Instruments Inc., Farmingdale, NY) or in two dimensions with a Slidex projector (Slidex Corp., Long Island City, NY). Molecular dimensions were measured from negatives enlarged to a final magnification of 560,000. Tip and base directions along axonemes were determined by markers such as the spoke period, A-microtubule extension at the tip, and basal body location. Micrographs showing surface views of straight axonemal regions were used to deduce the structure of the in situ arm.

Reactivation Methods: Study of the substructure of in situ outer dynein arms utilized demembranated sperm suspended in the reactivation buffer used for concurrent light microscopic observations. Sea urchins (*S. purpuratus*) were induced to shed sperm by KCl injection, and the sperm were stored on ice until needed. For reactivation studies, 20 μl of undiluted sperm were suspended in 1.5 ml of a demembranation buffer composed of 10 mM Tris-HCl pH 8.1, 2 mM $CaCl_2$, 0.15 M potassium acetate, 2 mM $MgSO_4$, 1 mM dithiothreitol, 0.1 mM EDTA, and 0.05% Triton X-100 (wt/vol). After 30 s the sample was diluted to 3 ml with a base reactivation buffer (10 mM Tris-HCl pH 8.1, 1 mM EDTA, 0.15 M potassium acetate, 2 mM $MgSO_4$, and 1 mM dithiothreitol), and the samples were gently sedimented into a loose pellet (Sorvall HB4 rotor, 4,000 rpm, 1.5 min). The supernate was replaced with a small volume of reactivation buffer (with or without ATP) being careful not to disturb the pellet. The demembranated sperm were immediately prepared for reactivation for separate but simultaneous light microscopic observation and freezing experiments as described below.

For light microscopy an aliquot of the loose pellet of cells was diluted into 2.5 ml reactivation buffer in petri dishes designed for dark field microscopic observations. ATP was added to produce a final $MgATP^{2-}$ concentration of 1 mM, and under these buffer conditions nearly 100% of the sperm were motile and beat at 34 Hz with symmetrical waveforms. Beat frequency was measured by synchronization with the Chadwick-Helmuth xenon strobe (Chadwick-Helmuth Co., El Monte, CA) coupled to a digital interval counter.

For freezing, a small aliquot of the loose pellet of demembranated sperm suspended in reactivation buffer with or without ATP was mounted as usual on thin slices of lung. (The lung slices had been previously washed in reactivation buffer and were shown, in separate experiments, not to affect the quality of reactivated sperm samples.) The mounted sample was then immediately frozen. In other experiments samples mounted in reactivation buffer devoid of ATP were sprayed with reactivation buffer containing 10 mM $MgATP^{2-}$ and frozen 3–5 s later. An artist's air brush, mounted on the freezing stand was used to apply the ATP solution. To verify that the ATP had reached the sample, hemocyanin was included in the ATP solution. Although the local ATP concentration in the sample at the time of freezing is unknown using this approach, it was determined in separate experiments that nearly 100% of the

demembranated, reactivated *S. purpuratus* sperm were motile and had symmetrical waveforms over a wide range of MgATP^{2-} concentrations (10^{-5}–10^{-2} M). Frozen samples were etched and replicated as described above.

It is of interest to note that some quick-frozen demembranated sperm could be thawed and then reactivated. In thawed samples, the sperm that remained physically intact could be reactivated to beat with the same frequency and waveform as control reactivated sperm that had not been frozen and thawed; however, most sperm were shattered and thereafter remained immotile.

Biochemical Procedures: Protein was determined by the method of Lowry et al. (30) using bovine serum albumin (BSA) as a standard. Gel electrophoresis was done in the presence of sodium dodecyl sulfate (Sigma-L-5750, Sigma Chemical Co., St. Louis, MO), 2-mercaptoethanol, and urea as described by Piperno and Luck (40). To best resolve the high molecular weight and intermediate molecular weight polypeptides of dynein fractions, the separating gels were 1.5-mm thick slabs composed of a 3–6% linear acrylamide gradient and 0–8 M urea gradient. Gels were run at constant voltage and stained either with Coomassie Brilliant Blue R-250 or by the silver method (34) with qualitatively identical staining patterns.

Deionized water was used throughout. Imidazole, Tris, BSA, glycine, dithiothreitol, and SDS were purchased from Sigma Chemical Co. Acrylamide and bis-acrylamide were purchased from Eastman Kodak Co. (Rochester, NY). All other reagents were analytical grade.

RESULTS

Polypeptide Composition

The polypeptide composition of the high-salt-extracted dynein-1 from axonemes of the sea urchin *S. purpuratus* was as previously reported for dynein-1 of other species (6). Fig. 1 illustrates the high molecular weight polypeptides of isolated axonemes (lane *A*), a crude high-salt extract (lane *B*), a 21S dynein-1 peak (lane *C*), and a 12S dynein peak (lane *D*). The 21S dynein-1 is comprised of the α- and β-heavy chains and three intermediate weight polypeptides, IC-1, -2, and -3, whose molecular weights are estimated to be 119,000, 92,000,
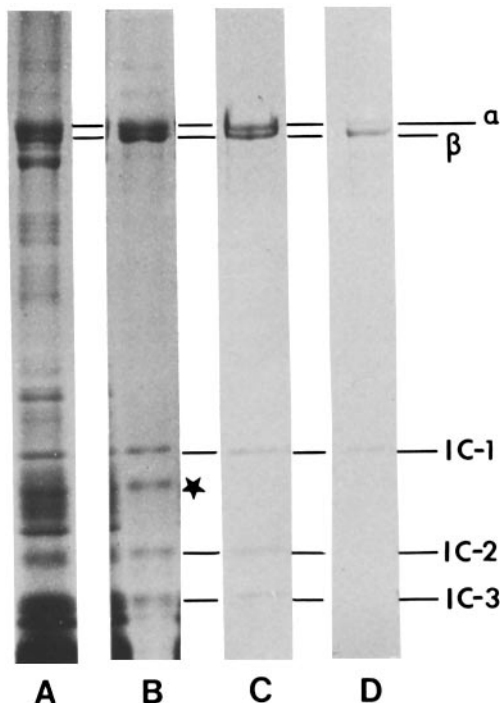

FIGURE 1   Lanes from a single SDS polyacrylamide slab gel of: (A) isolated axonemes; (B) fresh high-salt extract of axonemes; (C) sucrose gradient–purified 21S dynein-1; and (D) sucrose gradient–purified 12S dynein-1 subunit. The high-salt extract and 21S dynein-1 fraction contain α- and β-heavy chains (α and β) and IC-1, -2, and -3. The 12S dynein-1 subunit is comprised of the β-heavy chain and IC-1. ★, 105,000-D protein. Coomassie Blue stained.

and 75,000 D (the IC-1 chain often appears to be a doublet). The beta/IC-1 dynein-1 subfraction is comprised of the β-heavy chain, and the IC-1 polypeptide and is usually devoid of the α-heavy chain and IC-2 and -3; however, the fraction selected for lane *D* contains a small amount of the α-heavy chain. The crude high-salt extract has a very similar polypeptide composition to the 21S dynein-1 peak, indicating that the high-salt extract is largely composed of 21S dynein-1. One exception is a protein of ~105,000 D (Fig. 1 B, star). It is not known what structure this protein is associated with. It does not sediment with 21S dynein-1 in sucrose gradients.

The polypeptide distributions in the sucrose gradients used to purify 21S dynein-1 and its beta/IC-1 dynein-1 subunit are shown in more detail in Fig. 2. Fig. 2*A* is an image of the ATPase profile and polypeptide distribution of the sucrose-gradient fractions used to isolate 21S dynein-1. The ATPase peak (fraction *13*) is estimated to be 21S and coincides with the peak of dynein-1 polypeptide subunits, including α- and β-heavy chains (Fig. 2*A*, small arrowheads) and IC-1, -2, and -3 (large arrowheads). The 21S dynein-1 particle also contains light chains, but these have not been studied in detail. Inclusion of taxol in the high-salt extract buffer had no obvious effects on the sedimentation of 21S dynein-1 (data not shown).

Fig. 2*B* shows the ATPase profile and polypeptide distribution of fractions from the 9–16S region of a sucrose gradient designed to isolate the beta/IC-1 dynein-1 subunit. The ATPase peak (fraction *8*) sediments at ~12S and is composed of the β-heavy chain, IC-1, and trace amounts of two high molecular weight polypeptides that migrate slightly faster than the β-heavy chain. Under these gradient conditions, the ATPase peak rarely contains α-heavy chains that sediment between 15–30S (α in Fig. 2*B*) and is devoid of the IC-2, -3 polypeptides that sediment more slowly at 9–10S (Fig. 2*B*, fractions 6 and 7, small arrowheads).

Structure of Dynein-1

Freeze etch replicas of the fresh high-salt-extracted dynein-1 from sea urchin sperm axonemes reveal two-headed particles. Fig. 3 is a survey view of such a replica of fresh high-salt-extracted dynein-1 diluted to 20 μg/ml and adsorbed to mica and frozen as described in Materials and Methods. Particle types on exposed mica surfaces include a background of nonvolatile salts (Fig. 3, asterisk) and clusters of various numbers of large, distinct pear-shaped or spherical head-like structures (Fig. 3, arrows). We refer here to each of these large globular pear-shaped or spherical units as a head. The heads have very uniform replicated dimensions: spherical, ~14.5 nm in diameter; pear-shaped, ~18.5 × 12.5 nm. Such particles were never seen in control replicas of the buffers devoid of protein. For analysis we categorized the head-containing clusters into three groups: single-headed (example not included in Fig. 3), double-headed (Fig. 3, curved arrows), and irregular aggregates of three or more heads (Fig. 3, straight arrows). Out of 150 discrete, head-containing clusters in 20 μm^2 of replica, 23% were single-headed, 55% were double-headed, and 22% were irregular aggregates. Our criteria for classification of particles by head number were conservative. For 14 different fields of view analyzed (from four different replicas), it was necessary that single-headed and double-headed molecules were distinct, discrete units. Otherwise a particle cluster was categorized as an aggregate. For example the stars in Fig.
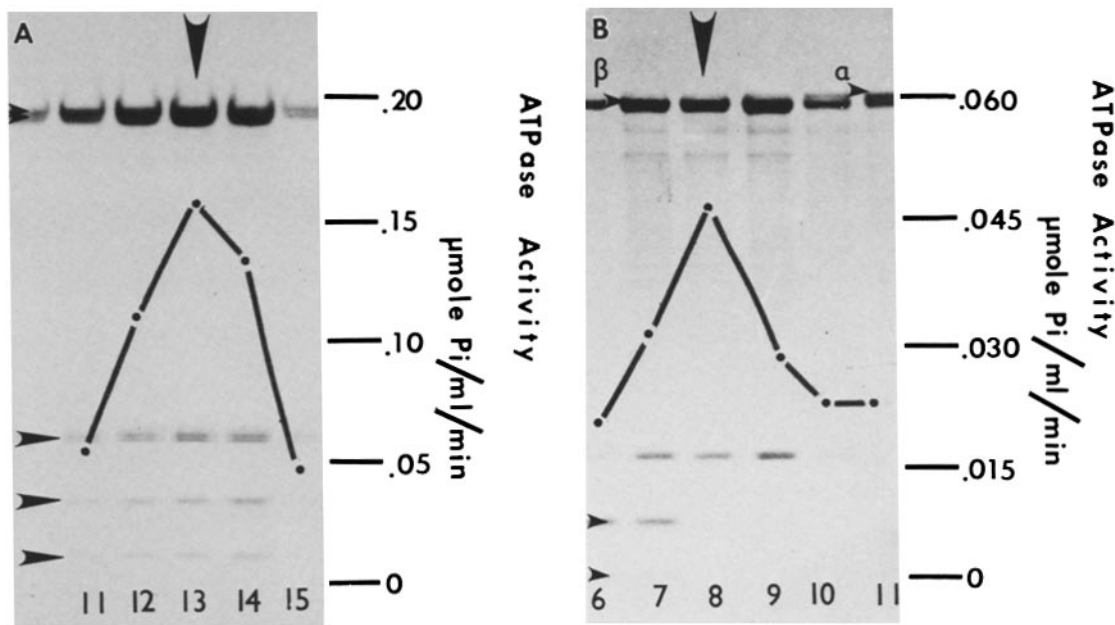
FIGURE 2 Characterization of sucrose gradient fractions by ATPase assay and SDS polyacrylamide gel electrophoresis. The direction of sedimentation was from left to right. A shows fractions from the 15–25S region of a sucrose gradient used to purify 21S dynein 1. The 21S peak, fraction 13, is composed of α- and β-heavy chains and IC-1, -2, and -3. From this gradient fractions 13 and 14 were pooled and dialyzed for 8 h against high-salt buffer to remove sucrose before electron microscopy. Note that IC-1 migrates as a doublet. B shows fractions from the 9–15S region of a sucrose gradient used to purify the 12S dynein-1 subunit. The ATPase peak, fraction 8, is comprised of the β-heavy chain and IC-1. This fraction was dialyzed against low-salt buffer to remove sucrose. (Note that lane 8 of B was underloaded and the β-heavy chain and IC-1 do not correlate with the ATPase peak. In all other correctly loaded gels [eight separate experiments] there is a direct correlation of ATPase and these two proteins.) Silver stained.

3 denote particle clusters within an aggregate that could be interpreted as two-headed particles. However, based upon our criteria these were counted in the aggregate. There were no clear examples of discrete three-headed particles in the replicas. Based upon their predominance we concluded that the two-headed structures represent the dynein-1 molecule and were analyzed further.

Fig. 4 is a gallery of molecules visualized by quick-freeze, deep-etch. Each of the two heads proves to be distinct in shape and size: one head is pear-shaped and measures 18.5×12.5 nm ($n = 56$; SD = 1.0 nm), and the other head is round and 14.5 nm in diameter ($n = 56$; SD = 1.0 nm). Of 122 two-headed molecules studied, 78% had morphologically distinguishable heads; in the remaining molecules, both heads appeared spherical, possibly because the pear-shaped particle was being viewed end-on, or possibly because a protein subunit was lost which would otherwise contribute to the pear-shaped head. (In Fig. 5a, a survey view of 21S dynein-1 particles on mica, the two-headed molecules happen to display spherical heads [arrows].) The heads adhere to the mica substrate in random orientations, in contrast to the three-headed outer arms from Chlamydomonas (18), and they are loosely joined by an irregular array of smaller subunits. As discussed in more detail below, the high-salt-containing extraction buffer appears to disrupt or loosen the molecule before mica adsorption, thereby obscuring structural details of the smaller subunits.

Fig. 5a shows a portion of a mica flake carrying particles from the 21S dynein-1 fraction. The replica reveals a mixture of two-headed molecules (arrows), single-headed molecules (squares), and clusters of three small bead-like subunits (cir-

cles). A selection of these prominent particle types is displayed in Fig. 6. The two-headed molecules (top row of Fig. 6) are comparable to those in the high-salt extract except that they tend to be even more disrupted and spread on the substrate. The heads are usually distinguishable and have the same dimensions as the pear-shaped and round heads of the two-headed molecules in Fig. 4. The heads of the single-headed molecules (middle row of Fig. 6) usually have the shape and dimensions of the pear-shaped head (18.5×12.5 nm); the stems of these particles carry a variable arrangement of smaller bead-like subunits. The third row of Fig. 6 shows the clusters of three subunits. The two lateral beads are spherical, and the central bead is larger and oblong. Based solely on morphological criteria, the three-bead clusters resemble the decorative material that binds the two heads together (Figs. 4 and 6, top) and projects from single-headed molecules. In particluar, there is a resemblance to the cluster indicated by the arrow in Fig. 4.

The beta/IC-1 dynein-1 subfraction contains single-headed molecules, and the heads are predominantly pear-shaped. Fig. 5b shows a representative region of a replicated mica flake displaying many single-headed molecules (circles). Of the discrete, globular particles in such fields, 68% ($n = 85$) were pear-shaped; the remainder were spherical. As noted above, spherical heads may be end-on views of pear-shaped heads since a definite pear-shape is detectable only 78% of the time in the intact two-headed protein; alternatively the extraction of a light chain or some other protein component may convert pear-shaped heads into spherical heads. (The pear-shaped head of isolated, shadowed myosin becomes spherical upon extraction of regulatory light chains [11].) A gallery of single-
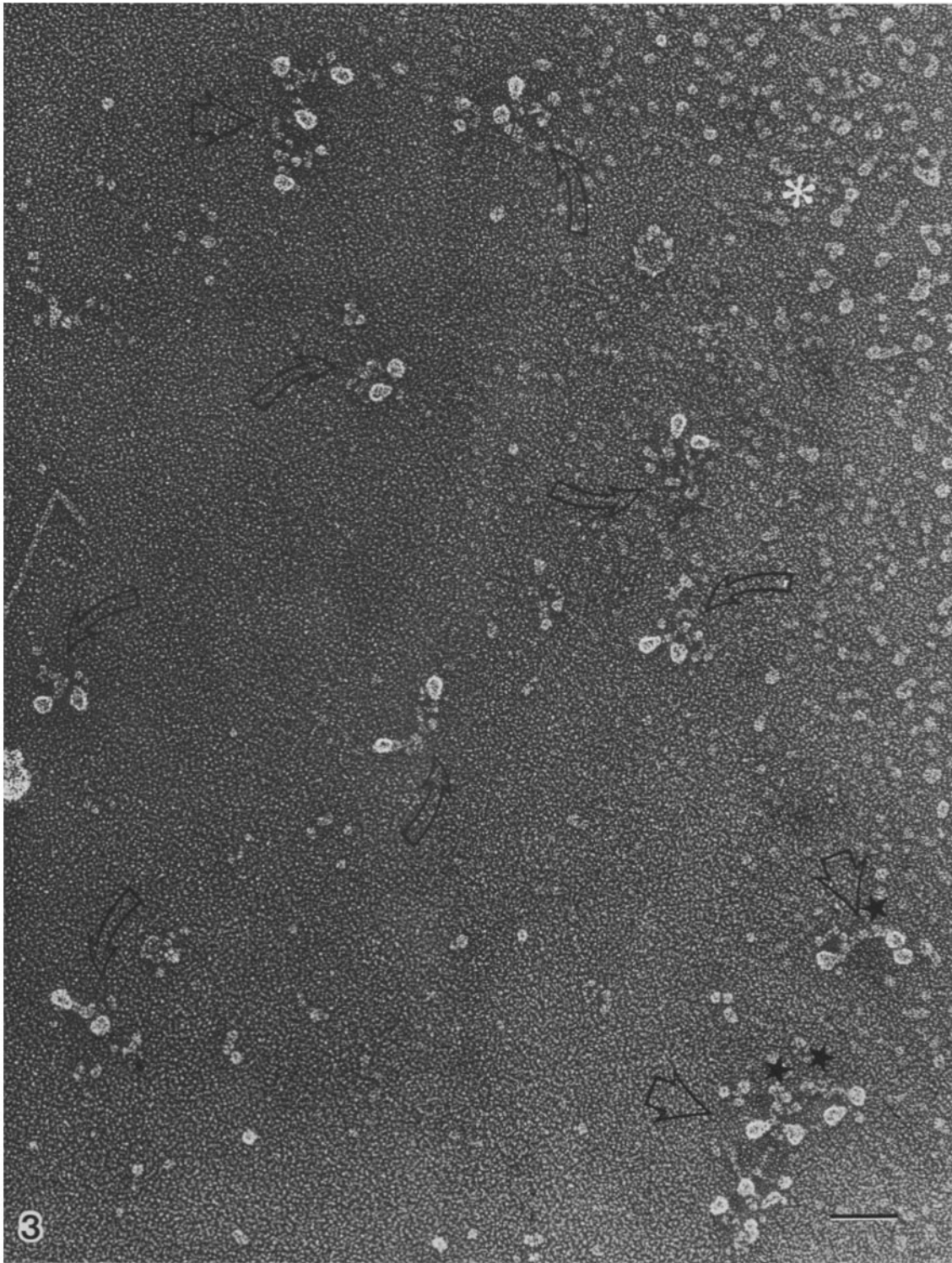
FIGURE 3 Survey view of a replica of the taxol-containing fresh high-salt extract of dynein-1 adsorbed to mica flakes (see Materials and Methods for details of freezing, etching, and shadowing). The predominant particles are two-headed proteins defined by the curved arrows. Stars denote possible two-headed particles within a large aggregate, and the asterisk marks a region of unidentified background particles. For description of analysis see Results. Bar, 50 nm. × 210,000.

headed molecules is displayed in Fig. 7. The pear-shaped heads have the same dimensions as the pear-shaped heads of the intact two-headed particles. A stem domain and associated bead-like subunits project from the narrow end of the head. The stem often ends in a pair of small globular subunits (Fig. 7, arrows).

Organization of Subunits in In Situ Outer Arms

Fig. 8, *a*, *b*, and *c* show micrographs of sea urchin axonemes that indicate possible relationships between the structure of the isolated two-headed dynein-1 and the structure of the in situ outer arm. Shown are examples in which the outer row
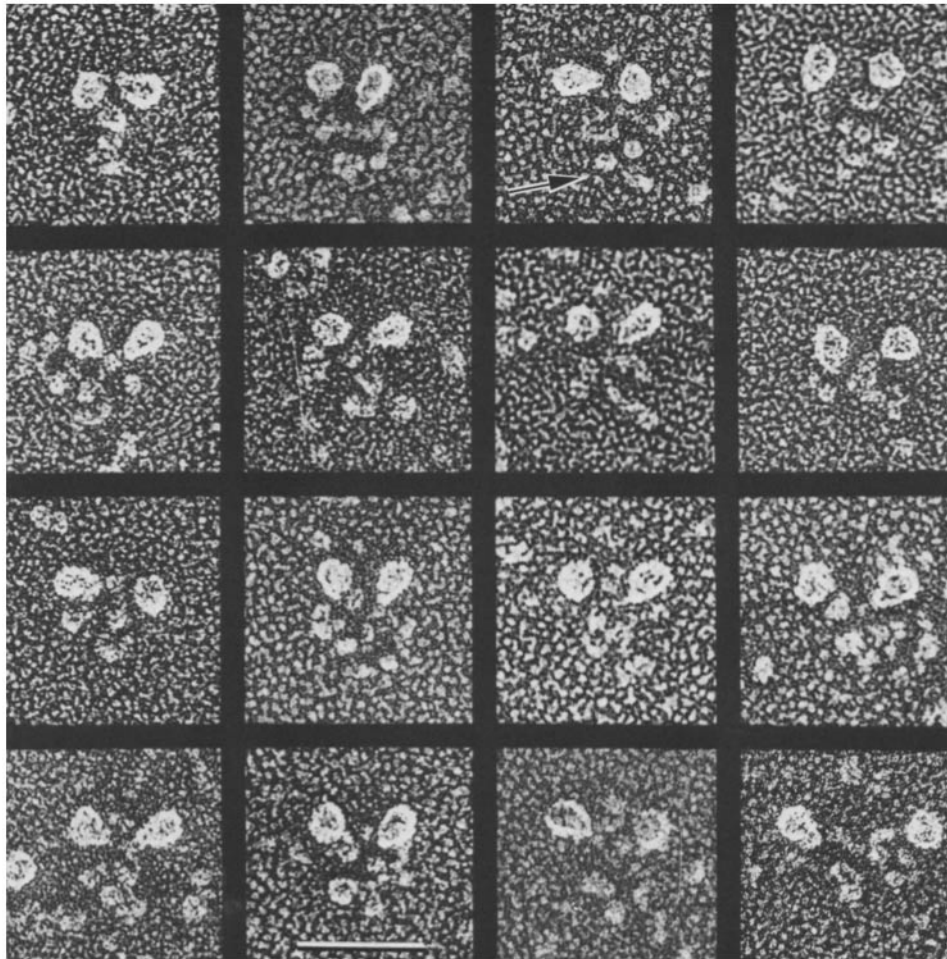
FIGURE 4 Representative two-headed proteins found in the fresh high-salt extract. The two heads of each protein can be distinguished as pear-shaped or spherical. The proteins appear to adsorb to the mica substrate in random orientation. Bar, 50 nm. × 350,000.

of arms has undergone either various degrees of spontaneous or high-salt extraction or microtubule splaying during sample preparation, since it has previously been shown that such disrupted axonemes yield particularly informative images (18). The images are arranged such that the distal tip of the axoneme is to the left. Fig. 8 a shows a row of outer dynein arms in lateral view. Prominent are globular heads that partially span the interdoublet gap. The large, globular heads repeat at 24 nm and are associated with smaller subunits (feet) that sit between adjacent globular heads and attach to the A-microtubule (arrowheads, Fig. 8 a). Although not evident in this micrograph, most heads are linked to the adjacent B-tubule by a thin stalk (see Fig. 8 d). This image of the outer dynein arm is generally consistent with that described earlier for protozoan cilia (17, 18).

As previously shown for protozoan outer arms (18), the in situ image viewed from the lateral perspective is misleading in that the outer-arm proteins in fact overlap one another. A diagram of the overlapped outer arms in sea urchin axonemes is presented in Fig. 9A, where each head is seen to make contact with two small subunits that are part of the molecule proximal to it. In Fig. 8 a, the arrowheads point to the prominent intervening subunit which is also indicated by arrow-

heads in the Fig. 9 diagram and is designated the P-foot (for proximal). The small distally displaced subunits are masked by overlying heads on the left side of Fig. 8 a. However, on the right side, two heads are missing at the positions marked by large arrows; as a result, the small subunits upon which they formerly rested are exposed (small arrows). A comparison of this region with the diagram in Fig. 9 B indicates that two entire outer-arm proteins are missing from the row at the positions marked by the arrows.

A more extreme example of this same phenomenon is given in Fig. 8 b, which shows an axoneme exposed to high salt such that most of its outer arms were extracted. The elongated configuration of the residual arms is evident. The perpendicular arrowheads again point to the intervening subunit, while the small white arrows indicate the firm attachment of the small subunits, the distal feet (D-feet) (Fig. 8 b), to the A-microtubule.

A final illustration of the overlapping arrangement of outer arms is given in Fig. 8 c. Here, doublets at the distal tip have begun to splay apart, causing each outer arm to stretch out of the overlapped position. The globular heads and associated stalks (arrowheads) have pulled away from the feet of their proximal neighbors.
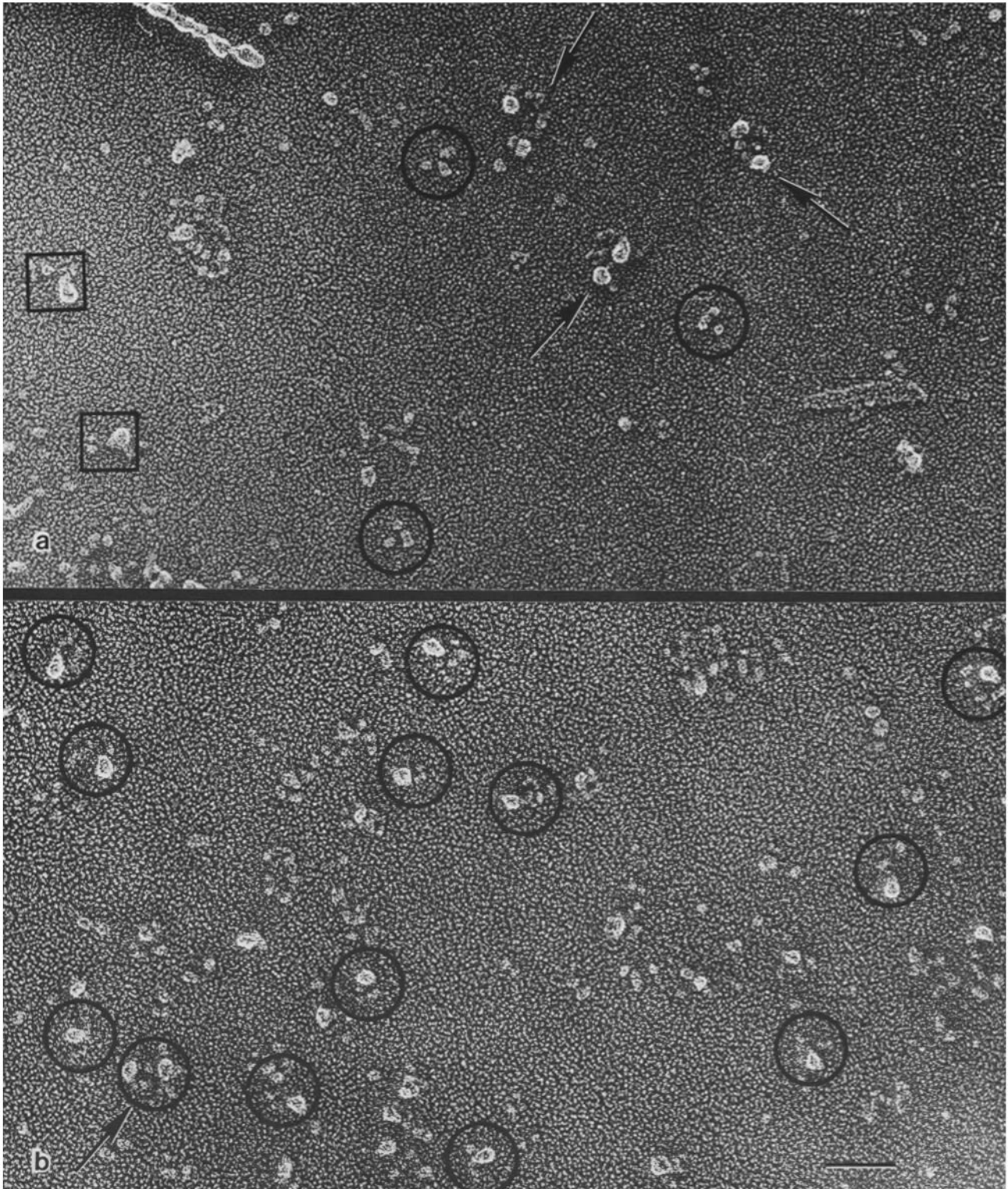
FIGURE 5 Low-power electron micrographs of replicas of quick-frozen, deep-etched proteins from (a) the dialyzed 21S dynein-1 fraction and (b) the dialyzed beta/IC-1 dynein-1 subfraction. The dialyzed 21S dynein-1 fraction contained three predominant particle types: two-headed proteins (arrows); single-headed proteins (boxes); and clusters of three small, globular subunits (circles). The beta/IC-1 dynein subfraction (b) contains single-headed proteins (circles). One particle appears to be two-headed (arrows in b). Other replicated particles have not been identified but may include nonvolatile salts (i.e., imidazole, EDTA, NaCl) and contaminating or distorted proteins (see reference 21). Bar, 50 nm. × 240,000.

Based upon an understanding that each outer dynein arm is attached to the A-microtubule distally by small subunits, the D-feet (D in Fig. 9A), and that the heads overlap the origin of the next proximal outer arm, it is possible to interpret the structure of nondisrupted, in situ outer arms in straight regions of the axoneme. Fig. 8d shows a row of outer arms
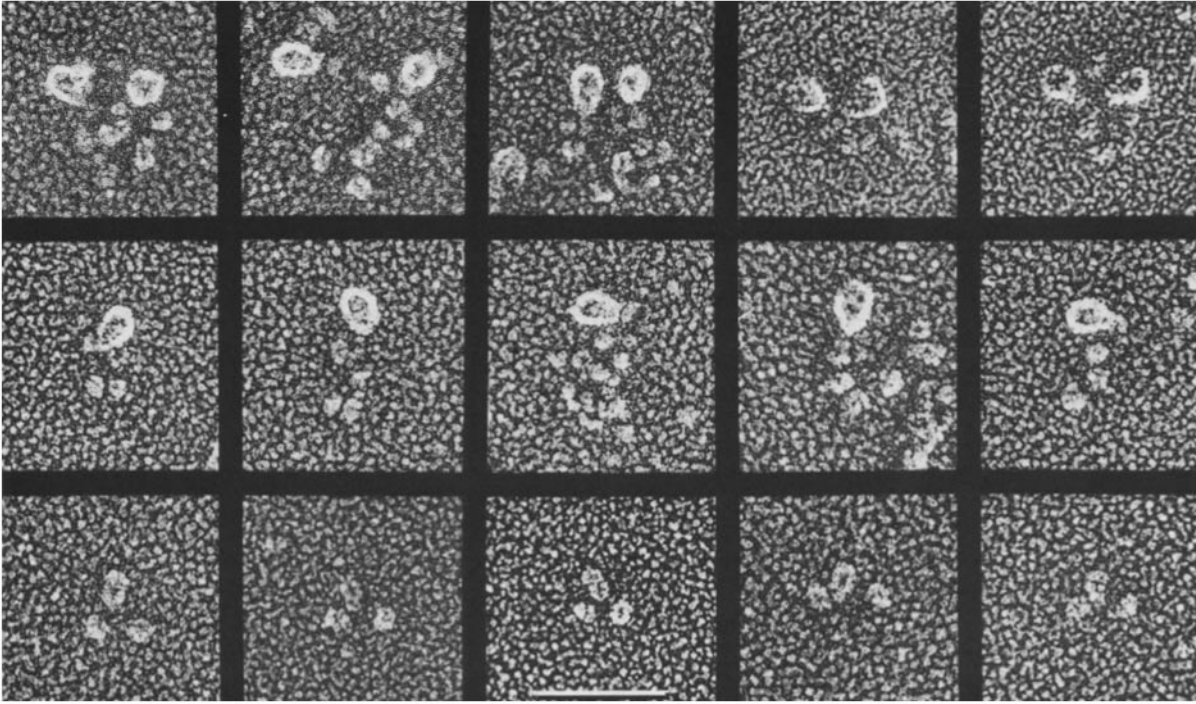
FIGURE 6 Particles from the dialyzed 21S dynein-1 fraction from a sucrose gradient. The prominent particles include two-headed proteins, single-headed proteins, and clusters of bead-like subunits. The two-headed particles are similar to those of the fresh high-salt extract (Fig. 3) in that they are comprised of a pear-shaped head and a spherical head. Bar, 50 nm. × 350,000.
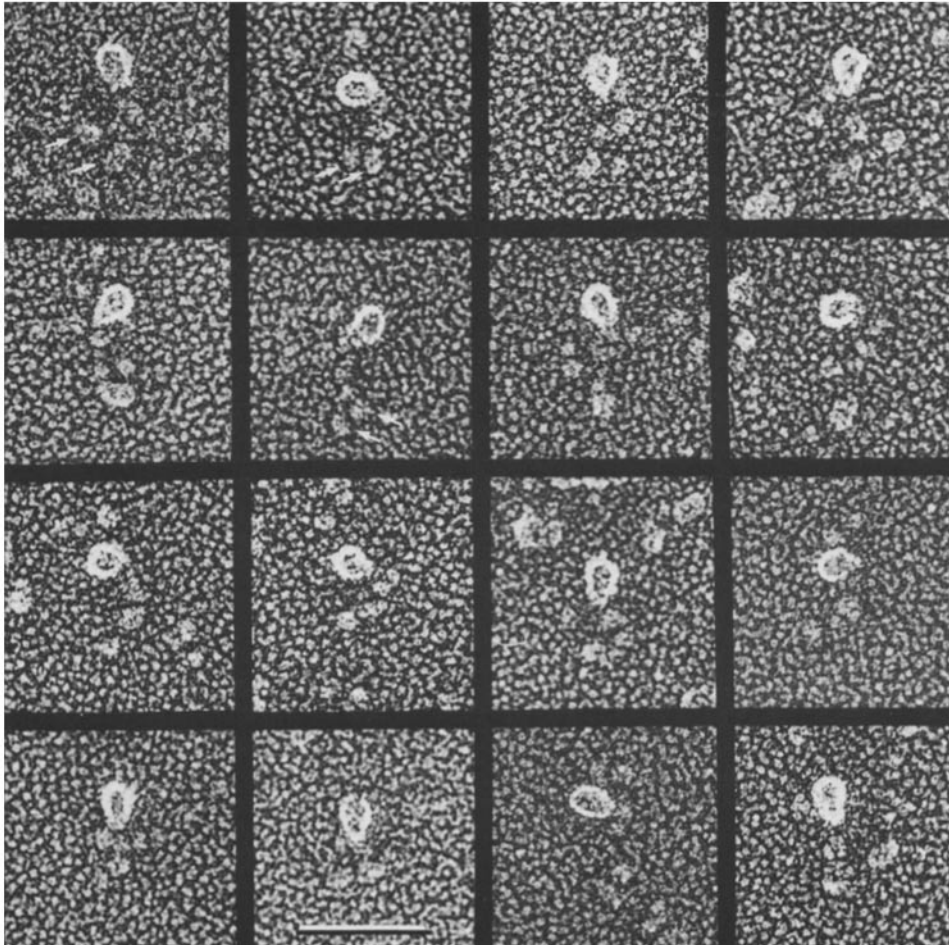
FIGURE 7 Single-headed molecules from the dialyzed beta/IC-1 dynein-1 subfraction from a sucrose gradient. The heads were generally the shape and dimensions of the pear-shaped head of the two-headed proteins. Bar, 50 nm. × 350,000.
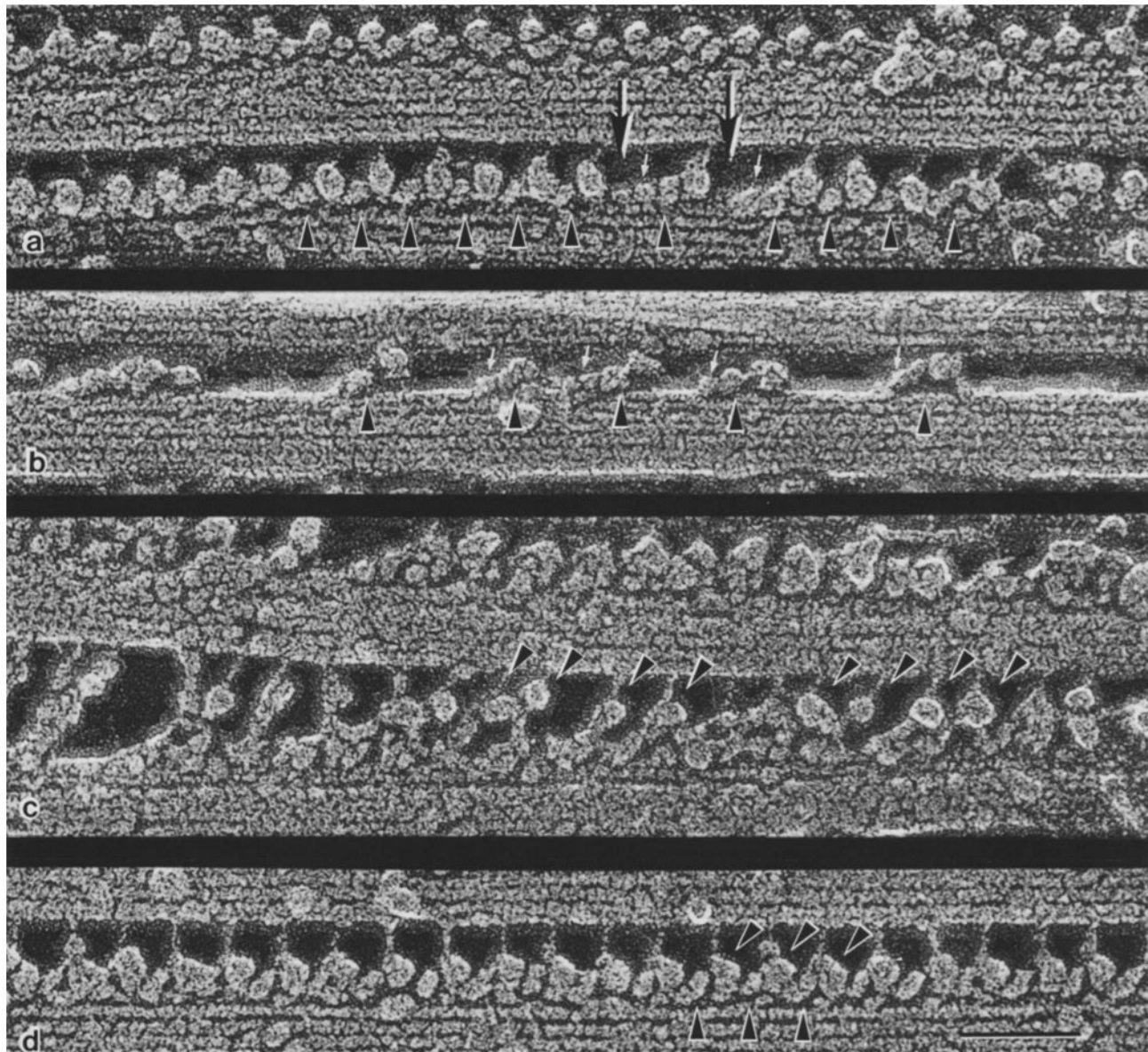
FIGURE 8 (a–c) Images of rotary-shadowed replicas of straight regions of axonemes in various states of disruption that optimally reveal in situ outer dynein arm subunit organization. The distal end of the axoneme is to the left. In a, a row of outer dynein arms is shown with two prominent gaps where arms are missing (arrows). Such partially extracted axonemes illustrate the substructure of the outer arm: each outer arm is attached distally by small globular feet (small arrows and arrowheads), and these globular feet are in turn linked to the large, proximally displaced globular heads. The large globular heads overlap the feet of the next proximal dynein arm. This slanted structure is clearly visualized in the outer arms which remain in high-salt-extracted axonemes (b). This arrangement is further illustrated in axonemes in which doublets have splayed apart and the stretched outer dynein arms extend out of the overlap position (c). In such splayed images it is clear that the dynein arms are attached to the A-microtubule by the distal end. In d, a region of an axoneme is shown frozen in reactivation buffer without ATP. Symbols are described in the text. Bar, 50 nm. × 350,000.

from a demembranated sperm suspended in reactivation buffer without added ATP, a condition of the sperm tail axoneme we define here as rigor (12, 17, 35). The bottom row of arrowheads denotes the P-feet associated with three outer arms (P in Fig. 9A). The upper row of tilted arrowheads denotes the three corresponding globular heads. The baseward slope of each protein, indicated by the cant of the tilted arrowheads, is ~35°. By contrast, the stalks are perpendicular to the microtubule surface, and they emanate from the distal portion of each head.

The outer dynein arms of sperm tail axonemes frozen in

reactivation buffer containing 1 mM ATP or sprayed with ATP-containing buffers (see Materials and Methods) have a very different structure from those of rigor sperm tail axonemes. The structure of the outer arm in ATP is very regular in straight regions of axonemes. As seen in Fig. 10, each unit consists of a large head that appears to be divided into two prominent globular domains, one above the other (Fig. 10, a–c, tilted arrows), a stalk emanating from the proximal side of these domains, and irregular intervening subunits (Fig. 10, b and c, downward arrows). Two parallel strands (Fig. 10, b and c, small horizontal arrows) can often be discerned extend-

RIGOR

A (D) (P) (H)

△ △ △

EXTRACT
SHADED
PROTEIN

B (D) (P) (H)

△ △ △

ATP

C (D) (P) (H) (D)

△ △ △

FIGURE 9 (A) Diagram of external view of rigor outer arm. The distal direction is to the left. Each outer arm is comprised of a large head (H) which is attached to the A-microtubule by smaller distally disposed subunits collectively referred to as the D-foot (D). The arrowheads denote P-feet (P) as the subunit interposed between heads. Each head overlaps the D-foot (D) of the next proximal outer arm, and the distal feet are hidden under the heads unless the adjacent dynein arms have been extracted, as in B and in Fig. 8, A and B. The two heads of each outer dynein arm are superimposed from this lateral view. (C) An interpretive diagram of the structure of outer arm exposed to ATP (see Fig. 10). The head is a bipartite structure, possibly because the two heads are now visible in lateral view. Parallel strands run between heads. The small intervening subunit (D) is possibly the same subunit as the hidden D-foot of rigor dynein arm, although this has not been directly demonstrated.

ing from one unit to the next.

Three salient differences distinguish the structure of the outer arms in the presence vs the absence of ATP. (a) In ATP, the globular head appears to be comprised of upper and lower domains, whereas in the absence of ATP the globular head does not display a division. (b) In ATP, the stalk emanates from the proximal aspect of the globular head, whereas in the absence of ATP the stalk projects from the distal end of the head. (c) In ATP, the region between adjacent heads is irregular in structure (Fig. 10, small white arrows), whereas without ATP there is a distinct intervening subunit (Fig. 8, a and d).

One interpretation of the ATP image is that the head viewed in rigor (Fig. 9A) rotates 90° revealing a bilobed head and intervening strands. Another interpretation of the ATP image is diagrammed in Figure 9C. We propose that in ATP, the prominent globular heads shift basally so that they lie over, and thereby shield, the P-foot (rather than the D-foot). Accompanying this shift is a rotation of the globular heads such that the single large head visible in the absence of ATP rotates to reveal its two domains. In other words, the two prominent globular domains revealed in such lateral views are interpreted to be the two molecular heads identified for the isolated dynein-1. The intervening subunit is interpreted to be the D-foot (whereas it is interpreted to be the P-foot in the rigor flagellar axoneme). Finally, there is a proximal shift in stalk position, presumably accompanying the shift in head orientation. These changes in outer arm structure parallel those

that have been proposed for protozoan outer arms in ATP (18).

A structure that we interpret as the 5–6 bridge is also displayed in Fig. 10a (large horizontal arrow). The bridge is a beaded structure with a regular 24-nm repeat. As opposed to the dynein arms, the bridge sits approximately equidistant from and between doublets, is attached to doublet 5 (lower) by short narrow trunks, and to doublet 6 (upper) by irregular narrow struts (many not visible in Fig. 10a). Adjacent globular elements are connected longitudinally by a narrow linker that is skewed toward doublet 6. A unit of this sort is never seen in cilia or flagella that do not reveal a bridge in cross-sections (17, 18).

DISCUSSION

Sea Urchin Dynein In Vitro

Fig. 11A summarizes the particle types analyzed in this paper and their polypeptide compositions. Although previous structural studies have indicated that sea-urchin sperm-tail dynein-1 might be two-headed (44, 60) and the Bell and Gibbons model (4) predicts a two-headed dynein from biochemical data, the images presented in this paper are the first to clearly document the presence of two heads. Recent modeling studies using Kirkwood-Bloomfield theory and data from Figs. 4 and 7 of this paper predict sedimentation coefficients of 21.2S and 12S for the two-headed dynein-1 and the single-headed beta/IC-1 subunit, respectively (Clutter, D., and K. A. Johnson, personal communication; and cf. reference 10. For calculation, molecular weights of 1.3 megadalton and 600,000 D were assumed for dynein 1 and the beta/IC-1 subunit, respectively, and a partial specific volume of 0.74 cm³/g used.) The micrographs also show that one of the heads is pear-shaped and the other spherical. Since dissociated dynein-1 yields a smaller 12S–14S particle with a pear-shaped head and a β-heavy chain, we conclude that the pear-shaped head is composed of the β-chain and, therefore, that the round head is composed of the α-chain.

A possibly unexpected consequence of dialyzing gradient-purified 21S dynein-1 against high salt is that many of the proteins dissociate into subunits. Particularly interesting in these preparations is the presence of clusters of three small bead-like subunits (Fig. 6), which bear a strong resemblance to a cluster of three subunits decorating the intact protein (Fig. 4, arrow). We are presently exploring the posssibility that this cluster might correspond to the 9–10S species containing IC-2 and -3 that migrates as a stable particle in sucrose gradients (55). Such a model would be consistent with that of Bell and Gibbons (4) in which the IC-2 and -3 particle comprises a portion of the A-microtubule binding site.

A comparison of dynein-1 from sea urchin with quick-frozen images of Chlamydomonas and Tetrahymena dyneins (18) indicates that all are constructed on the same head-stem plan. There are, however, differences, the most obvious being that the protozoan dyneins have three heads (18, 28, 59), whereas sperm-tail dynein has two. In a recent preliminary report, Marchese-Ragona et al. (32) found bull sperm 18S dynein to be two-headed, and 21S dynein-1 from the sea urchin Tripneustes gratilla, when studied by scanning transmission electron microscopy, is also a two-headed protein (Gibbons, I. R., and K. A. Johnson, personal communication). It will clearly be interesting to learn whether two-headed outer arms prove to be a diagnostic feature of sperm dyneins.
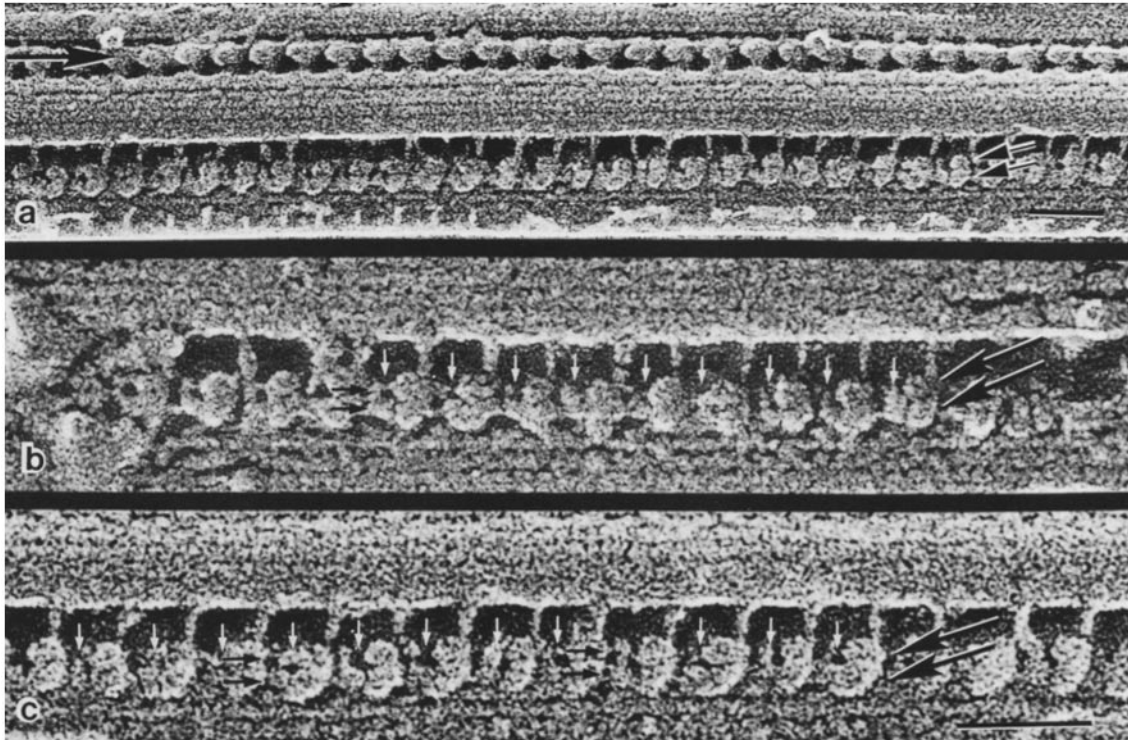
FIGURE 10 Straight regions of sperm tail axonemes frozen in reactivation buffer containing ATP. Representative longitudinal views of outer arms are displayed. Notably the head displays two globular domains (tilted arrows in a–c) and the stalks emanate from the proximal end of each head and project to the B-microtubule of the adjacent doublet. Also included is a periodic structure interpreted to be the 5–6 bridge (horizontal arrow in a). Bar, 50 µm. (a) × 200,000. (b and c) × 350,000.

Since there is no evidence that outer dynein arms of these sperm have a third head, the purpose of the third head in protozoan dyneins is not known. However, there is biochemical and genetic data suggesting that the outer arms of *Chlamydomonas* are comprised of three heavy chains (25, 37, 40) and that each heavy chain is associated with ATPase activity (36, 38); there is also biochemical and kinetic evidence that favor three sites of ATPase activity in the outer arm dynein from *Tetrahymena* (26, 51). Similarly, each of the α- and β-heavy chains of sea urchin outer arm dynein is associated with ATPase activity (55). Therefore, the simplest conclusion based upon composition, structure, and mass analysis is that each head is an ATPase-containing unit, with three heads and heavy chains in the outer dynein arms of *Chlamydomonas* and *Tetrahymena*, and two heads and heavy chains in the outer dynein arms of sea urchin sperm flagella.

Examination of Fig. 4 indicates that the stem domains vary considerably in morphology from one protein to the next: some are quite compact, others appear extremely loose and disorganized. Studies with *Chlamydomonas* dynein demonstrate that variability in structure can be generated by exposure to high salt, since such variability is minimized when the outer arms are released from doublets by exposure to high concentrations of ATP (18). Unfortunately, we have been unable to extract sea-urchin dynein using ATP, and therefore cannot detail how its stem decoration is organized.

Sea Urchin Dynein In Situ

Previous studies of deep-etched protozoan outer arms in situ have shown the presence of two feet, the D-foot and the

P-foot, associated with the A-microtubule, and the probable presence of a tripartite head. One unit of the head rests on its neighbor's D-foot and the second rests on its neighbor's P-foot, giving the head an oblong, mallet shape; the third head unit lies behind the other two and is not normally visible (17, 18).

In the sea-urchin sperm tail, entities corresponding to a D-foot and a P-foot can be identified in arms of rigor sperm tails, although their shapes and sizes are different from their protozoan counterparts (Figs. 8 and 9). Presumably the intervening subunit (Fig. 8, vertical arrowheads) corresponds to the P-foot, and the D-foot is hidden under the heads. The key difference between the two images in rigor axonemes is that whereas a globular head unit of the sea urchin outer arm rests on its neighbor's D-foot, no globular head unit is associated with the neighboring P-foot, so that each P-foot stands exposed as the prominent intervening subunit identified by the arowheads in Fig. 8, a, b, and d. Furthermore, the intervening subunit is larger and located more proximal relative to the heads of each dynein arm, compared with the P-foot in the protozoan outer arms. Knowing that sea-urchin dynein-1 is comprised of two head units in vitro, we must assume that in rigor axoneme, one globular head lies behind the other as drawn in Fig. 9, A and B and 11 B. This general model of outer dynein arm structure is consistent with other electron microscopic data (2, 18, 58) and with models developed from mass distribution analysis by scanning transmission electron microscopy of dynein bound to microtubules (28). Furthermore, this arrangement of the heads would account for the hook-shaped outer dynein arm viewed in cross-sections (1,

HSE

plus taxol

21S FRACTION

dialyzed
(high salt)

12S FRACTION

dialyzed
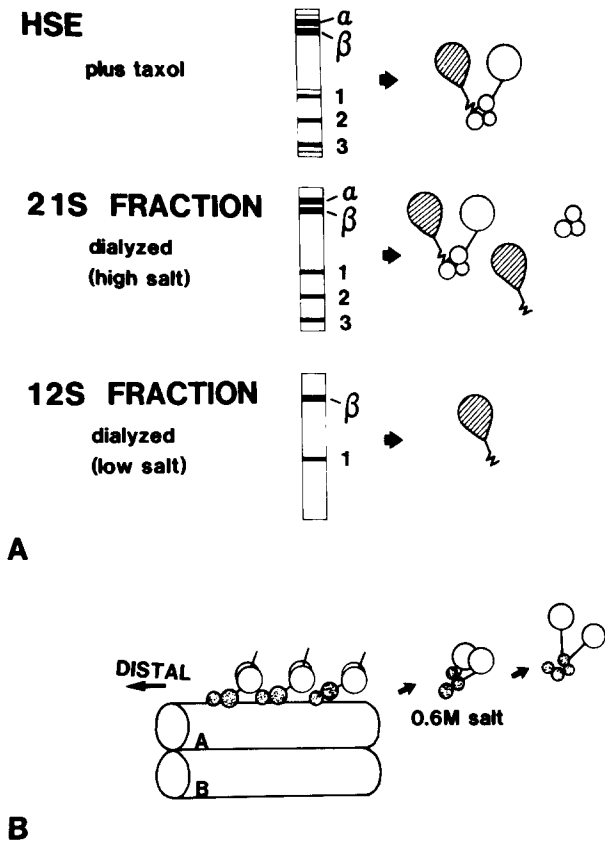(low salt)

A

DISTAL

0.6M salt

B

FIGURE 11 (A) Summary diagram of polypeptide composition and particle types in the dynein fractions described in Results. We conclude that the two-headed particle is the 21S dynein-1 molecule. (B) General model of outer dynein arms of sea urchin sperm axonemes, and one interpretation of the relationship of the general structure of the outer arm and the extracted two-headed dynein. The outer arm is comprised of a head which attaches to the A-microtubule by small, distally disposed subunits (feet) and attached to the adjacent B-microtubule (not illustrated) by a thin stalk.

cance of these changes in head position is unclear at present. One interpretation is that these structural changes represent distinct states of a cyclic cross-bridge cycle. However, it is curious that, at least in straight segments of rapidly frozen reactivated sea urchin sperm, each outer arm appears identical in conformation to its neighbor. One might have expected to see a systematic or random change in macromolecular structure associated with the capture of dynein arms in transitions associated with the cross-bridge cycle. It is possible that flagellar axonemes were immotile at the time of freezing. It is also possible that the freezing step is relatively slow and actually captures a rate-limiting step in a cross-bridge cycle or that in actively bending axonemes, cycling force-generating arms are localized to bent regions and/or specific subsets of doublet microtubules. Future studies will focus on a comparison of outer-arm structure in straight and bent regions of rapidly frozen, reactivated flagellar axonemes.

21, 27). Similar general models of outer dynein arm structure have been presented (5, 27, 29).

As suggested from biochemical data (36), it is possible that the heavy chains of 18S dynein from *Chlamydomonas* are equivalent to the heavy chains of 21S dynein-1 from sea urchin, since they share several fractionation properties. If so, then the missing molecular head in sea urchin, or the extra molecular head in protozoa, may correspond to the unit comprised of the γ-heavy chain and this unit may be equivalent to the proximal globular head present in the protozoan rigor arm but absent from the sperm rigor arm. By this reasoning, α- and β-heavy chains would correspond to the distal head and the hidden head (or the reverse) in all three organisms. Obviously the situation may be more complex than this, and in situ antibody labeling of individual structures will be required to resolve the issue.

The fact that two large globular domains are visible in each outer arm when sea-urchin axonemes are exposed to ATP is interpreted to mean that the hidden head and the visible head both rotate and twist ~90° when ATP is present (see Fig. 9 C). A similar kind of head rotation was proposed to explain the ATP image in protozoan axonemes (18). Both heads, moreover, appear to shift proximally in ATP, again as appears to occur in protozoan axonemes (18). However, the signifi-

REFERENCES

1. Allen R. D. 1968. A reinvestigation of cross-sections of cilia. *J. Cell Biol.* 37:825–831.
2. Avolio, J., S. Lebduske, and P. Satir. 1984. Dynein arm substructure and the orientation of arm-microtubule attachments. *J. Mol. Biol.* 173:389–401.
3. Bell, C. W. 1983. The molecular weight of dynein chains. *J. Submicrosc. Cytol.* 15:201–202.
4. Bell, C. W., and I. R. Gibbons. 1982. Structure of dynein 1 outer arm in sea urchin sperm flagella. II. Analysis by proteolytic cleavage. *J. Biol. Chem.* 257:516–522.
5. Bell, C. W., and I. R. Gibbons. 1983. Preparation and properties of dynein ATPase. *Muscle and Nonmuscle Motil.* 2:1–36.
6. Bell, C. W., E. Fronk, and I. R. Gibbons. 1979. Polypeptide subunits of dynein 1 from sea urchin sperm flagella. *J. Supramol. Struct.* 11:311–317.
7. Bell, C. W., C. Fraser, W. Sale, W.-J. Tang, and I. R. Gibbons. 1982. Preparation and purification of dynein. *Methods Enzymol.* 85:405–474.
8. Brokaw, C. J. 1972. Flagellar movement: a sliding filament model. *Science (Wash. DC).* 178:455–462.
9. Cande, Z., and S. Wolniak. 1978. Chromosome movement in lysed mitotic cells is inhibited by vanadate. *J. Cell Biol.* 79:573–580.
10. Clutter, D., D. Stimpson, V. Bloomfield, and K. Johnson. 1983. The structure of *Tetrahymena* dynein in solution. *J. Cell Biol.* 97 (5, Pt. 2):197a. (Abstr.)
11. Flicker, P., T. Wallimann, and P. Vilbert. 1983. Electron microscopy of scallop myosin. Location of regulatory light chains. *J. Mol. Biol.* 169:723–741.
12. Gibbons, B. H., and I. R. Gibbons. 1974. Properties of flagellar "rigor waves" formed by abrupt removal of adenosine triphosphate from actively swimming sea urchin sperm. *J. Cell Biol.* 63:970–985.
13. Gibbons, B. H., and I. R. Gibbons. 1979. Relationship between the latent adenosine triphosphatase state of dynein 1 and its ability to recombine functionally with KCl-extracted sea urchin sperm flagella. *J. Biol. Chem.* 254:197–201.
14. Gibbons, I. R. 1981. Cilia and flagella of eukaryotes. *J. Cell Biol.* 91:107–124.
15. Gibbons, I. R., and E. Fronk. 1979. A latent adenosine triphosphatase form of dynein 1 from sea urchin sperm flagella. *J. Biol. Chem.* 254:187–196.
16. Goodenough, U. W. 1983. Motile detergent-extracted cells of *Tetrahymena* and *Chlamydomonas*. *J. Cell Biol.* 96:1610–1621.
17. Goodenough, U. W., and J. E. Heuser. 1982. The substructure of the outer dynein arm. *J. Cell Biol.* 95:798–815.
18. Goodenough, U. W., and J. E. Heuser. 1984. Structural comparison of purified proteins with *in situ* dynein arms. *J. Mol. Biol.* 180:1083–1118.
19. Goodenough, U. W., and J. E. Heuser. 1985. Substructure of inner dynein arms, radial spokes, and the central pair/projection complex. *J. Cell Biol.* 100:2008–2018.
20. Goodenough, U. W., and J. E. Heuser. 1985. Outer and inner dynein arms of cilia and flagella. *Cell.* 41:341–342.
21. Haimo, L. T., B. R. Telzer, and J. L. Rosenbaum. 1979. Dynein binds to and cross-bridges cytoplasmic microtubules. *Proc. Natl. Acad. Sci. USA.* 76:5759–5763.
22. Heuser, J. 1983. Procedure for freeze-drying molecules adsorbed to mica flakes. *J. Mol. Biol.* 169:155–195.
23. Hisanaga, S., and M. M. Pratt. 1984. Calmodulin interaction with cytoplasmic and flagellar dynein: calcium-dependent binding and stimulation of adenosine triphosphatase activity. *Biochemistry* 23:3032–3037.
24. Hisanaga, S., and H. Sakai. 1983. Cytoplasmic dynein of the sea urchin egg. II. Purification, characterization, and interactions with microtubules and Ca-calmodulin. *J. Biochem. (Tokyo).* 93:87–98.

25. Huang, B., G. Piperno, and D. J. L. Luck. 1979. Paralyzed flagella mutants of *Chlamydomonas reinhardtii* defective for axonemal doublet microtubule arms. *J. Biol. Chem.* 254:3091-3099.

26. Johnson, K. A. 1983. The pathway of ATP hydrolysis by dynein. Kinetics of a presteady state phosphate burst. *J. Biol. Chem.* 258:13825-13832.

27. Johnson, K. A. 1985. Pathway of the microtubule-dynein ATPase and the structure of dynein: a comparison with actomyosin. *Annu. Rev. Biophys. Biophys. Chem.* 14:161-188.

28. Johnson, K. A., and J. S. Wall. 1983. Structure and molecular weight of the dynein ATPase. *J. Cell Biol.* 96:669-678.

29. Johnson, K. A., M. E. Porter, and T. Shimizu. 1984. Mechanism of force production for microtubule-dependent movements. *J. Cell Biol.* 99 (1, Pt. 2):132s-136s.

30. Lowry, O. H., N. J. Rosebrough, A. L. Farr, and R. J. Randall. 1951. Protein measurement with the folin phenol reagent. *J. Biol. Chem.* 193:265-275.

31. Luck, D. J. L. 1984. Genetic and biochemical dissection of the eukaryotic flagellum. *J. Cell Biol.* 98:789-794.

32. Marchese-Ragona, S. P., M. Belles Isles, C. Gagnon, J. S. Wall, and K. A. Johnson. 1984. Structures and masses of 14S dynein from *Tetrahymena* cilia and 19S dynein from bull sperm. *J. Cell Biol.* 99 (4, Pt. 2):45a. (Abstr.)

33. Martin, R. G., and B. N. Ames. 1964. A method for determining the sedimentation behavior of enzymes: application to protein mixtures. *J. Biol. Chem.* 236:1372-1379.

34. Morrisey, J. H. 1981. Silver stain for proteins in polyacrylamide gels: a modified procedure with enhanced uniform sensitivity. *Anal. Biochem.* 117:307-310.

35. Okuno, M. 1980. Inhibition of sea urchin sperm flagella by vanadate. *J. Cell Biol.* 85:712-725.

36. Pfister, K. K., and G. B. Witman. 1984. Subfractionation of *Chlamydomonas* 18S dynein into two unique subunits containing ATPase activity. *J. Biol. Chem.* 259:12072-12080.

37. Pfister, K. K., R. Fay, and G. Witman. 1982. Purification and polypeptide composition of dynein ATPases from *Chlamydomonas* flagella. *Cell Motil.* 2:525-547.

38. Pfister, K. K., B. E. Haley, and G. B. Witman. 1984. The photoaffinity probe 8-azidoadenosine 5'-triphosphate selectivity labels the heavy chain of *Chlamydomonas* 12S dynein. *J. Biol. Chem.* 259:8499-8504.

39. Piperno, G. 1984. Monoclonal antibodies to dynein subunits reveal the existence of cytoplasmic antigens in sea urchin egg. *J. Cell Biol.* 98:1842-1850.

40. Piperno, G., and D. J. L. Luck. 1979. Axonemal adenosine triphosphatases from flagella of *Chlamydomonas reinhardtii*. *J. Biol. Chem.* 254:3084-3090.

41. Porter, M., and K. Johnson. 1983. Transient state kinetic analysis of the ATP-induced dissociation of the dynein-microtubule complex. *J. Biol. Chem.* 258:6582-6587.

42. Pratt, M., T. Otter, and E. Salmon. 1980. Dynein-like Mg^{++}-ATPase in mitotic spindles isolated from sea urchin embryos. *J. Cell Biol.* 86:738-745.

43. Sakai, H., I. Mabuchi, S. Shimoda, R. Kuriyama, K. Ogawa, and H. Mohri. 1976. Induction of chromosome motion in the glycerol isolated mitotic apparatus: nucleotide

44. Sale, W. S. 1983. Low-angle rotary-shadow replication of 21S dynein from sea urchin sperm flagella. *J. Submicrosc. Cytol.* 15:217-223.

45. Sale, W. S., and P. Satir. 1977. Direction of active sliding of microtubules in *Tetrahymena* cilia. *Proc. Natl. Acad. Sci. USA.* 74:2045-2049.

46. Sale, W. S., U. Goodenough, and J. E. Heuser. 1984. The structure of dynein 1 of sea urchin sperm tail axonemes. *J. Cell Biol.* 99 (4, Pt. 2):44a. (Abstr.)

47. Satir, P. 1968. Studies on cilia. III. Further studies on the cilium tip and a "sliding filament" model of ciliary motility. *J. Cell. Biol.* 39:77-94.

48. Satir, P., and W. S. Sale. 1977. Tails of *Tetrahymena*. *J. Protozool.* 24:498-501.

49. Satir, P., J. Wais-Steider, S. Lebduska, A. Nasr, and J. Avolio. 1981. The mechanochemical cycle of the dynein arm. *Cell Motil.* 1:303-327.

50. Scholey, J., B. Neighbors, J. E. McIntosh, and E. D. Salmon. 1984. Isolation of microtubules and a dynein-like Mg ATPase from unfertilized sea urchin eggs. *J. Biol. Chem.* 259:6516-6525.

51. Shimizu, T., and K. Johnson. 1983. Kinetic evidence for multiple dynein ATPase sites. *J. Biol. Chem.* 258:13841-13846.

52. Shingyoji, C., A. Murakami, and K. Takahashi. 1977. Local reactivation of Triton-extracted flagella by iontophoretic application of ATP. *Nature (Lond.).* 265:269-270.

53. Summers, K., and I. R. Gibbons. 1971. Adenosine triphosphate-induced sliding of tubules in trypsin-treated flagella of sea urchin sperm. *Proc. Natl. Acad. Sci. USA.* 68:3092-3096.

54. Takahashi, M., and Y. Tonomura. 1978. Binding of 30S dynein with the B-tubule of the outer doublet of axonemes form *Tetrahymena p.* and adenosine triphosphate-induced dissociation of the complex. *J. Biochem. (Tokyo).* 84:1339-1355.

55. Tang, W.-J. Y., C. W. Bell, W. S. Sale, and I. R. Gibbons. 1982. Structure of the dynein-1 outer arm in sea urchin sperm flagella. I. Analysis by separation of subunits. *J. Biol. Chem.* 257:508-515.

56. Tsukita, S., S. Tsukita, and J. Usukura, and H. Ishikawa. 1983. ATP-dependent structural changes of the outer dynein arm in *Tetrahymena* cilia: a freeze-etch replica study. *J. Cell Biol.* 96:1480-1485.

57. Warner, F. D., and D. Mitchell. 1978. Structural conformation of ciliary dynein and the generation of sliding forces in *Tetrahymena* cilia. *J. Cell Biol.* 76:261-277.

58. Witman, G. B., and N. Minervini. 1982. Dynein arm conformation and mechanochemical transduction in the eukaryotic flagellum. *In Eukaryotic and Prokaryotic Flagella.* W. B. Amos and J. G. Duckett, editors. *Symp. Soc. Exp. Biol.* 35:203-223.

59. Witman, G. B., K. A. Johnson, K. K. Pfister, and J. S. Wall. 1983. Fine structure and molecular weight of the outer dyneins of *Chlamydomonas*. *J. Submicrosc. Cytol.* 15:193-198.

60. Yano, Y., and T. Miki-Noumura. 1981. Two-headed dynein arm. *Biomed. Res.* 2:73-78.

specificity and effects of anti-dynein and myosin sera on motion. *Dev. Growth. & Differ.* 18:211-219.